Vol.3, No.2, 111-126 (2012)
http://dx.doi.org/10.4236/jbpc.2012.32013

Journal of Biophysical Chemistry

A B3LYP study on electronic structures of $[(X)_mMn(\mu\text{-oxo})_2Mn(Y)_n]^{q+}$ (X, Y = H_2O, OH and O) as a Mn cluster model of OEC

Masashi Katsuda, Masaki Mitani, Yasunori Yoshioka*

Chemistry Department for Materials, Graduate School of Engineering, Mie University, Tsu, Japan;
*Corresponding Author: yyoshi@chem.mie-u.ac.jp

Received 14 December 2011; revised 19 January 2012; accepted 6 February 2012

ABSTRACT

Electronic and molecular structures of $[(X)_mMn(\mu\text{-oxo})_2Mn(Y)_n]^{q+}$ (X, Y = H_2O, OH and O), which are Mn cluster models at catalytic sites of OEC, were studied by broken-symmetry unrestricted B3LYP method. Two paths from the S_0 to S_3 states of Kok cycle were investigated. One is a path starting from [Mn(II) (μ-oxo)$_2$Mn(III)] at the S_0 state, and another is from [Mn(III) (μ-oxo)$_2$Mn(III)] at S_0. Results found in this study are summarized as, 1) In [Mn(II), Mn(III)], it is not possible that H_2O molecules coordinate to the Mn atoms with retaining the octahedral configuration. 2) The OH^- anion selectively coordinates to Mn(IV) rather than Mn(III). 3) When the oxo atom directly bind to the Mn atom, the Mn atom must be a Mn(IV). From these results, the catalytic mechanism for four-electron oxidation of two H_2O molecules in OEC is proposed. 1) The Mn_4(II, III, IV, IV) at S_0 is ruled out. 2) For Mn_4(III, III, IV, IV) at S_1, the Mn atom coordinated by OH^- anion is a Mn(IV) not Mn(III). 3) Only Mn(III) ion which is coordinated by a H_2O molecule at S_0 plays crucial roles for the oxidation.

Keywords: Oxygen Evolving Complex; Manganese Binuclear; Oxidation Mechanism

1. INTRODUCTION

Manganese atoms play important roles in the oxygen-evolving complex (OEC) of photosystem II, the catalytic site for the four-electron oxidation of water to molecular oxygen such as $2H_2O \rightarrow O_2 + 4e^- + 4H^+$. Kok and co-workers have proposed, known as Kok cycle, that the oxidation proceeds through five states denoted as from S_0 to S_4 under four times of irradiation of light and remove of four protons [1]. Recently, the structures of OEC have been reported by the X-ray crystallographic studies [2-5]. Four manganese atoms and calcium ion are present at the catalytic site. The manganese atoms and calcium ion are arranged in cubanelike geometry with Mn_2O_2 face of the di-μ-oxo-bridged [Mn(μ-O)$_2$Mn]. The Mn-Mn distances were observed to be about 2.7 for Mn_2O_2 face [6-9].

As shown in **Figure 1**, three electrons and two protons are released from the catalytic site during the oxidation from S_0 to S_3. The molecular oxygen is formed from S_3 through unstable S_4 by releasing an electron and two protons. The oxidation states of the four Mn atoms at the S_0 state have been suggested as Mn_4(II, III, IV, IV) or Mn_4(III, III, III, IV) [10-16]. Even if the oxidation states of four manganese atoms at S_0 are different, the oxidation states change as Mn_4(III, III, IV, IV) at the S_1 state $\rightarrow$ Mn_4(III, IV, IV, IV) at S_2 $\rightarrow$ Mn_4(III, IV, IV, IV) at S_3 $\rightarrow$ Mn_4(III, IV, IV, IV) at S_4. However, the oxidation states of four manganese atoms and ligand state at S_3 are still under debate. Two possibilities have been mostly discussed [17-22]: 1) Mn-centered oxidation; 2) oxidation of water molecule forming Mn-O or Mn-OH bonds as a direct Mn-ligand.

In the 1990s, binuclear bis(μ-oxo)dimanganese complexes [(L_m)Mn(μ-O)$_2$Mn(L'_n)] were prepared and characterized [23-33]. For many complexes, the ligands comprise bi- and/or tri-dentate compounds with lone pair electrons of nitrogen and oxygen atoms. The mixed valence [Mn(III)(μ–O)$_2$Mn(IV)] complexes, which was expected to correspond to the S_2 state of OEC, were intensively examined, since EXAFS and EPR studies suggest short Mn–Mn distance of ~2.7 Å and a multiline signal at g ~ 2, respectively [34-36]. It was thought from the spectroscopic studies of OEC that the catalytic site contains the $[Mn_2O_2]^{3+}$ core. However, the process of H_2O oxidation could not be recognized from the model complexes, since the models do not contain H_2O, OH^- and O^{2-} (oxo) as ligands connecting directly to the manganese atoms.

In accordance with experimental works, theoretical works of the [(L_m)Mn(μ-O)$_2$Mn(L'_n)] complexes were performed by using density functional methods and broken-symmetry (BS) procedure for the low-spin states [37-39].

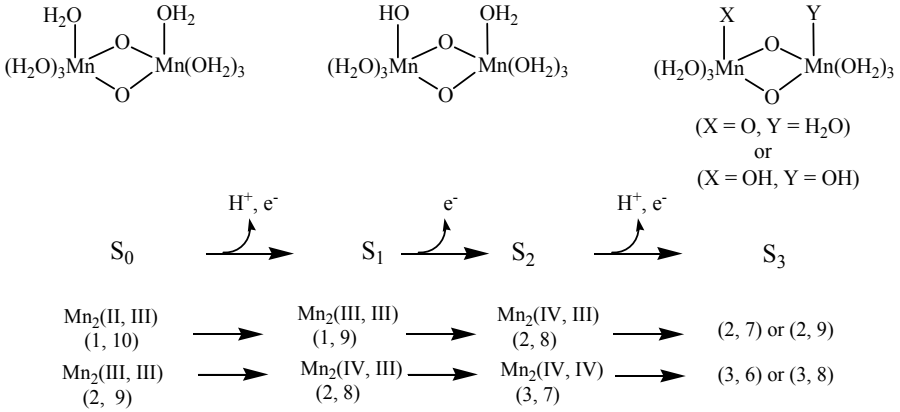

Figure 1. Schematic representation from S_0 to S_3 states corresponding to Kok cycle. Values in parenthesis denote total charge and spin multiplicity for high spin states.

The [Mn(III)(μ-O)$_2$Mn(IV)] complexes were mostly concentrated to investigate the geometries and spin-spin coupling constants of two manganese atoms in order to compare with experimental observations [37-43]. Small model [Mn(μ-O)$_2$Mn] complexes where NH_3, H_2O and μ-oxo directly bind to manganese atom were also examined for the iso-valence Mn(II)/Mn(II), Mn(III)/Mn(III) and Mn(IV)/Mn(IV) and mixed valence Mn(II)/Mn(III), Mn(III)/Mn(IV) and Mn(IV)/Mn(V) [44-49]. However, these small models were discussed without strict relationship to the catalytic states in Kok cycle.

[$(H_2O)_4$Mn(μ-O)$_2$Mn$(H_2O)_4$] complex is a most fundamental model of the S_0 state of catalytic site [49,50]. This model has the possibility to present the intermediate S_1, S_2 and S_3 states where the proton(s) is(are) released from the H_2O molecule. **Figure 1** shows schematically the expected changes of the oxidation states for two Mn atoms and (total charge and spin multiplicity) of the Mn_2O_2 core through from S_0 to S_3 states in the Kok cycle. From the proposals that the oxidation states of four Mn atoms are assigned as Mn_4(II, III, IV, IV) or Mn_4(III, III, III, IV) at the S_0 state, it is reasonable to assume that the oxidation states of two Mn atoms are Mn_2(II, III) or Mn_2(III, III) at S_0. If we assume that the oxidation proceeds through the release of an electron from Mn atoms at each step, for the high spin state of Mn_2(II, III) at the S_0 state, the electronic state changes as (1, 10) at S_0 → (1, 9) at S_1 → (2, 8) at S_2. For Mn_2(III, III), it changes as (2, 9) at S_0 → (2, 8) at S_1 → (3, 7) at S_2. It is apparent that the S_2 state of Mn_2(II, III) series is perfectly same as the S_1 state of Mn_2(III, III) series. For the S_2 → S_3 transition, (2, 9) and (2, 7) are possible at S_3 for the Mn_2(II, III) series, while (3, 8) and (3, 6) are possible for the Mn_2(III, III) series. At this stage, the spin state of Mn_2 depends on the electronic structure of the formed Mn-O and Mn-OH bonds. To our knowledge, the experimental and theoretical studies of [Mn(μ-O)$_2$Mn] complexes with direct Mn-OH bonds are not found.

In our previous work [49], we focused on geometries and electronic structures of binuclear manganese complexes, $[(H_2O)_3Mn(\text{-}O)(\mu\text{-}O)_2Mn(OH_2)_4]^{q+}$ (q = 2 and 3), in which μ-oxo directly binds to Mn atoms as model complexes of the S_3 state. Investigated in the present work are geometries, energetic and electronic structures of the high and low spin states of the $[(H_2O)_4Mn(\mu\text{-}O)_2Mn(OH_2)_4]^{q+}$ (q = 1 or 2) complexes corresponding to S_0, $[(H_2O)_3(HO)Mn(\mu\text{-}O)_2Mn\text{-}(OH_2)_4]^{q+}$ (q = 1 - 3) to S_1 and S_2, and $[(H_2O)_3(HO)\text{-}Mn(\mu\text{-}O)_2Mn(OH)(OH_2)_3]^{q+}$ (q = 2 and 3) and $[(H_2O)_2\text{-}(HO)_2Mn(\mu\text{-}O)_2Mn(OH_2)_4]^{q+}$ (q = 2 and 3) to S_3. Examination is performed by using broken symmetry density functional methods for the low spin (LS) state and usual unrestricted method for high spin (HS) states. The oxidation states of two manganese atoms are determined and the spin coupling constants in the complexes are estimated. Finally, the possible oxidation mechanism of H_2O molecules at the catalytic site of OEC is discussed by combining the current results with previous results [49].

2. COMPUTATIONAL DETAILS

The complexes including single OH ligand have axial and equatorial configurations of the Mn-OH bonds for the [Mn(μ-O)$_2$Mn] face, as shown in **Figure 2**. The first character in the symbol (a, •) shows configuration of a ligand on the left side of two manganese atoms, while second one shows a ligand on the right side. Here we assign the left and right sides of two Mn atoms as Mn_a and Mn_b. Then, the symbol (a, •) means that OH binds to the Mn_a atom in axial configuration and the Mn_b atom has no OH ligand and has only H_2O ligands. The complexes including two OH ligands have a large number of combinations of OH configurations. The pre-character *t* and *c* of *t*-(a,a) and *c*-(a,a) shown in **Figure 2** means *trans* and *cis* configurations of two OHs binding to different Mn atoms, respectively. For the $[(H_2O)_3(HO)Mn\text{-}(\mu\text{-}O)_2Mn(OH)(OH_2)_3]$ complexes, independent configurations are

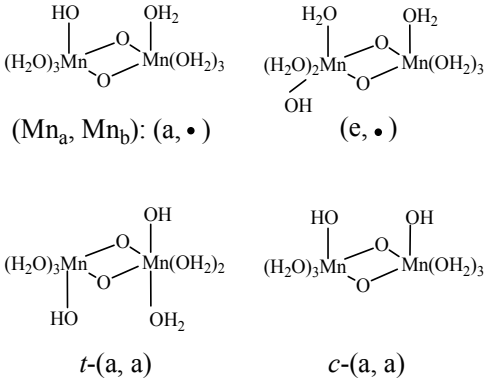

Figure 2. Notation of OH-configurations in the complexes. Symbol (a, •) means that Mn_a on the left side is coordinated by OH in axial configuration and Mn_b on the right side is coordinated by only H_2O molecules. Symbols *t* and *c* means *trans* and *cis* configurations, respectively.

t-(a,a), *c*-(a,a), *t*-(e,e), *c*-(e,e) and (e,a). For the $[(H_2O)_2(HO)_2Mn(\mu\text{-}O)_2Mn(OH_2)_4]$ complexes, three (aa, •), (ee, •) and (ae, •) configurations are independent.

The geometries of these configurations were fully optimized without any geometry constraints for the LS and HS states with all possible total charges shown in **Figure 1**. For the stationary geometries, the vibrational frequency analyses were carried out to confirm that the stationary point is a local minimum on potential energy surface. The usual unrestricted Hartree-Fock (UHF) method leads to poor estimations for the binuclear systems because of lack of the electron correlation effects in the transition metals. The hybrid exchange-correlation functional B3LYP method [51,52] was most widely used for the transition-metal systems. Since the B3LYP method contains the moderate static correlation effects, we employed the B3LYP method to estimate the electronic structures. The usual unrestricted method was used for the HS states, while the broken symmetry (BS) method was used for the LS states. The Ahlrichs DZV [53] and 6-31G* [54] basis sets were employed for Mn atom and for O and H atoms, respectively. After the optimized geometries were determined, the single point calculations were carried out using the Ahlrichs TZV [55] basis set for the Mn atom. Mulliken population analysis was used to estimate the distributions of spin densities. In this report, energies and spin densities estimated by TZV are summarized in Tables. All calculations were performed using the Gaussian 03 program package [56].

The transformation of the BS solution to first-order density matrix ($\hat{\gamma}^{(1)}$) gives the natural orbitals (NOs: $\phi_{\pm i}$) with their occupation numbers of electrons ($n_{\pm i}$), which provide a powerful tool to analyze the electronic structures of the LS states of binuclear systems and to determine the oxidation states of two Mn atoms

$$\hat{\gamma}^{(1)} = \sum_{i}^{N_\beta}\left(n_{-i}\left|\phi_{-i}\right\rangle\left\langle\phi_{-i}\right| + n_{+i}\left|\phi_{+i}\right\rangle\left\langle\phi_{+i}\right|\right) + \sum_{i}^{N_\alpha - N_\beta}\left|\phi_i\right\rangle\left\langle\phi_i\right| \quad (1)$$

where

$$n_{-i} + n_{+i} = 2 \text{ and } 1 \le n_{-i} \le 2 \quad (2)$$

N_α and N_β are numbers of up- and down-spins, respectively. Although the BS solution has the spin contamination $\left\langle \hat{S}^2 \right\rangle_{SC}$ to the spin angular momentum, it can be related to the occupation numbers of electrons ($n_{\pm i}$) in $\hat{\gamma}^{(1)}$ such as

$$\left\langle \hat{S}^2 \right\rangle_{SC} = \left\langle \hat{S}^2 \right\rangle_{BS} - \left\langle \hat{S}^2 \right\rangle_{Pure} = \sum_{i}^{N_\beta} n_{-i} n_{+i} \quad (3)$$

Here, $\left\langle \hat{S}^2 \right\rangle_{Pure}$ is the spin angular momentum of the corresponding pure spin state ($S = \left(N_\alpha - N_\beta\right)/2$). If the spins in ϕ_{-i} and ϕ_{+i} are antiferromagnetically coupled, the $n_{-i}n_{+i}$ values are nearly equal to unity with the relation of $n_{-i} + n_{+i} = 2$ $\left(n_{-i} \ge n_{+i} > 0\right)$. Thus, the $\left\langle \hat{S}^2 \right\rangle_{SC}$ value represents the number of the antiferromagnetic spin couplings in the system.

The NOs ϕ_{-i} and ϕ_{+i} are usually distributed over the binuclear with bonding and antibonding characters. The magnetic molecular orbitals (MMOs: $\psi_{\pm i}$), which are transformed from NOs as

$$\psi_{\mp i}(r) = \sqrt{\frac{n_{-i}}{2}}\phi_{-i}(r) \pm \sqrt{\frac{n_{+i}}{2}}\phi_{+i}(r) \quad (4)$$

present the distribution of the electron spin localized on Mn atom. Thus, from $\left\langle \hat{S}^2 \right\rangle_{SC}$ and $\psi_{\pm i}$, the oxidation states of Mn atoms and characteristic of spin coupling between two Mn atoms can be easily determined. The MMOs $\psi_{\pm i}$ are essentially same as the corresponding orbitals proposed by Amos and Hall [57].

Many procedures are defined for the (bi-)radical characters in the LS states. As an alternative way, the index of the (bi-)radical character for the antiferromagnetically coupled ϕ_{-i} and ϕ_{+i} can be defined by using the Shannon entropy theory [58,59]. For the BS solution,

$$\eta_i^{BS} = 1 - \frac{1}{2}\left(n_{-i}\log_2 n_{-i} + n_{+i}\log_2 n_{+i}\right) \quad (5)$$

Although the BS solution suffers from the spin contamination, the projection to the pure spin state can be easily carried out by using the paired MMOs ψ_{-i} and ψ_{+i}.

$$\Psi_i^{PBS} = \frac{1}{\sqrt{2\left(2 - n_{-i}n_{+i}\right)}}\left(\left\|\psi_{-i}\overline{\psi}_{+i}\right\| - \left\|\overline{\psi}_{-i}\psi_{+i}\right\|\right) \quad (6)$$

This equation can be rewritten by using the paired NOs ϕ_{-i} and ϕ_{+i}.

$$\Psi_i^{PBS} = \frac{n_{-i}}{\sqrt{n_{-i}^2 + n_{+i}^2}}\left\|\phi_{-i}\overline{\phi}_{-i}\right\| - \frac{n_{+i}}{\sqrt{n_{-i}^2 + n_{+i}^2}}\left\|\phi_{+i}\overline{\phi}_{+i}\right\|. \quad (7)$$

The spin projected first-order density matrix can be

constructed by using **Eq.8** and the index of the spin projected (bi-)radical character is defined as

$$\eta_i^{\mathrm{PBS}} = -\frac{n_{-i}^2}{n_{-i}^2+n_{+i}^2}\log_2\frac{n_{-i}^2}{n_{-i}^2+n_{+i}^2} - \frac{n_{+i}^2}{n_{-i}^2+n_{+i}^2}\log_2\frac{n_{+i}^2}{n_{-i}^2+n_{+i}^2} \quad (8)$$

3. RESULTS AND DISCUSSION

Computational results for all optimized geometries are summarized in **Tables S1**, **S2** and **S3** as supporting materials. **Table S1** summarizes the oxidation states, spin angular momentums and relative energies for all optimized geometries starting from Mn_2(III, II) at the S_0 state, while **Table S2** summarizes the results for all optimized geometries starting from Mn_2(III, III) at the S_0 state. **Table S3** summarizes the effective exchange integrals of the lowest LS states in energy. In text, low-lying configurations of them are discussed as well as the previous ones with the Mn = O bond [49].

3.1. S_0-S_2 States

Figure 3 shows optimized geometries of LS states from S_0 to S_2 states derived from Mn_2(II, III) and Mn_2(III, III) at S_0. The corresponding HS states have similar geometries to the LS states. **Table 1** summarizes the oxidation states of Mn atoms, spin contaminations, relative energies and spin coupling constants for the LS and HS states. **Tables 2** and **3** summarize the selected interatomic distances and spin densities of selected atoms, respectively.

Two LS states **1** and **3** are assumed to be Mn_2(III, II) and Mn_2(III, III) at the S_0 state, respectively. For the optimized state **1** in **Table 1**, $\langle S^2 \rangle_{SC}$ = 3.9923 indicates that the doublet state **1** has four antiferromagnetic pairs of spins localized on two Mn atoms and the natural orbital analysis indicates that unpaired single spin is localized on the Mn_b atom. Accordingly, the oxidation state of Mn atoms in the doublet state **1** is apparently assigned as Mn_2(III, II). The oxidation state of Mn_2(III, II) can be also confirmed by the spin densities of two Mn atoms, –3.783 and 4.715 e shown in **Table 3**. The Mn-Mn distance is given by 2.724 Å, comparable with 2.7 Å in the crystal structure of the active site of OEC. However, as can be seen from **Figure 3**, the coordinations of water molecules are remarkably deformed from octahedral configuration of Mn atoms. Two μ-oxo atoms shift to the Mn(III) ion. Differences of bond distances of Mn(III)-μO and Mn(II)-μO are given by 0.235 and 0.264 Å (**Table 2**). The decet state **2**, which is 2.3 kcal mol^{-1} above the doublet state **1**, has similar spin densities of 3.788 and 4.761 e on the Mn_a and Mn_b atoms to the state **1**, respectively, showing that the decet state **2** is obviously the HS state corresponding to the LS doublet state **1**.

For singlet state **3**, $\langle S^2 \rangle_{SC}$ = 3.9978 shows that the state **3** has four antiferromagnetic pairs of spins localized

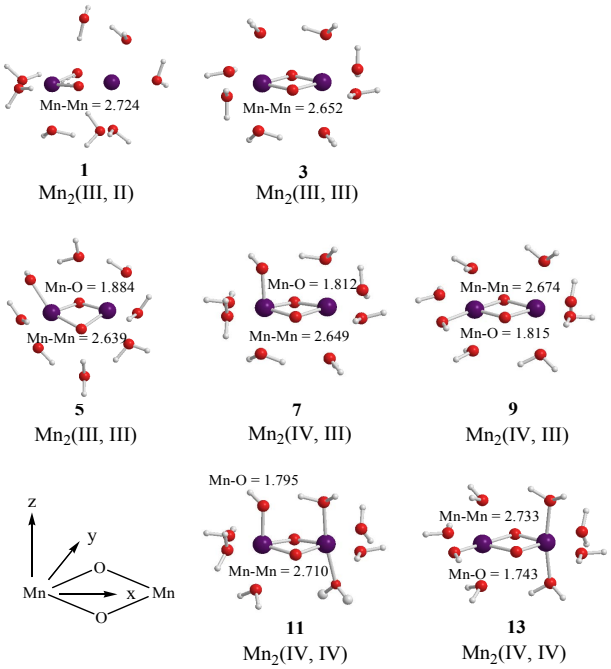

Figure 3. Optimized geometries of LS states from S_0 to S_2 states derived from Mn_2(II,III) and Mn_2(III,III) at S_0. Mn-Mn and Mn-O(OH) distances are shown in unit of Å.states. Tables 2 and 3 summarize the selected interatomic distances and spin densities of selected atoms, respectively.

on two Mn atoms. Thus, the oxidation states of two Mn atoms in the state **3** are apparently assigned by Mn_2(III, III). From **Figure 3**, the Mn–Mn distance is given by 2.652 Å, slightly shorter than 2.7 Å estimated by X-ray crystallographic study. However, coordination of water molecules is pseudo-octahedral configuration with high symmetry, in contrast with the doublet state **1** of Mn_2(III, II). The corresponding HS state **4** is 6.9 kcal·mol^{-1} higher than the state **3**.

It can be predicted from the crystal structure of OEC that four Mn atoms are coordinated by pseudo-octahedral configurations. It is, therefore, expected that the oxidation states of Mn atoms at the S_0 state is Mn_2(III, III) rather than Mn_2(III, II). In other word, it is thought that Mn_4(II,III,IV,IV) at the S_0 state in OEC can be ruled out.

When single OH^- anion coordinates to Mn atom at the S_1 and S_2 states shown in **Figure 1**, axial and equatorial configurations are possible. As shown in **Figure 1**, the expected oxidation states of two Mn atoms are Mn_2(III, III), Mn_2(IV, III) and Mn_2(IV, IV). Obtained was the LS singlet state **5** shown in **Figure 3**, which is thought to correspond to the S_1 state with Mn_2(III, III) oxidation states. The ligand OH^- anion is definitely deformed from axial configuration, although we set up an initial geometry in axial configuration before optimizing the geometry. Two Mn atoms are not strictly coordinated by H_2O molecules and OH^- anion in octahedral configuration. The OH^- anion is located at middle position between axial and

equatorial configurations. The Mn–Mn distance is given by 2.639 Å shorter than 2.7 Å of OEC. The BS solution of **5** has $\langle S^2 \rangle_{SC}$ = 4.0029, indicating that the oxidation state of Mn atoms is Mn_2(III, III), consistent with spin densities of 3.791 and –3.796 e shown in **Table 3**. We tried to obtain the optimized equatorial geometry of the OH^- anion by starting from equatorial configuration. However, the equatorial geometry was not obtained by approaching to the geometry **5**. Accordingly, it could be considered from these results that the oxidation state of Mn atom coordinated by the OH^- anion is not Mn(III), even the OH^- anion is generated as an intermediate through the oxidation of water molecules in OEC. Reversely, the ligand coordinating to Mn(III) is not a OH^- anion.

As shown in **Figure 1**, the respective S_2 and S_1 states derived from Mn_2(III, II) and Mn_2(III, III) at S_0 are expected to be common Mn_2(IV, III). For both LS and HS states, axial and equatorial geometries were optimized as

Table 1. Oxidation states, spin contaminations, relative energies and effective exchange integrals of the optimized **1-14** states estimated at B3LYP/TZV//B3LYP/DZV level.

States	Ligands[a]	Conf.[b]	Charges[c]	Spin states	Oxidation states	$\langle S^2 \rangle_{SC}$	ΔE_{rel}[d]	J_{Mn-Mn}[e]
		S_0 states						
1	(•, •)		1	Doublet	(III, II)	3.9923	0.0	–41
2	(•, •)		1	Decet	(III, II)	0.0463	2.3	
3	(•, •)		2	Singlet	(III, III)	3.9978	0.0	–150
4	(•, •)		2	Nonet	(III, III)	0.0887	6.9	
		S_1 states from Mn_2(III, II) at S_0						
5	(OH, •)	(a, •)	1	Singlet	(III, III)	4.0029	0.0	–108
6	(OH, •)	(a, •)	1	Nonet	(III, III)	0.0884	5.6	
	(OH, •)	(e, •)	1	Singlet	(III, III)	n.a.	n.a.	n.a.
	(OH, •)	(e, •)	1	Nonet	(III, III)	n.a.	n.a.	n.a.
S_2 and S_1 states from Mn_2(III, II) and Mn_2(III,III) at S_0, respectively								
7	(OH, •)	(a, •)	2	Doublet	(IV, III)	3.0141	0.0	–142
8	(OH, •)	(a, •)	2	Octet	(IV, III)	0.1061	4.4	
9	(OH, •)	(e, •)	2	Doublet	(IV, III)	2.9857	13.7	–150
10	(OH, •)	(e, •)	2	Octet	(IV, III)	0.0936	14.0	
		S_2 states from Mn_2(III, III) at S_0						
11	(OH, •)	(a, •)	3	Singlet	(IV, IV)	3.0568	0.0	–68
12	(OH, •)	(a, •)	3	Septet	(IV, IV)	0.1403	1.3	
13	(OH, •)	(e, •)	3	Singlet	(IV, IV)	2.9908	11.8	–87
14	(OH, •)	(e, •)	3	Septet	(IV, IV)	0.1061	13.5	

a) Symbol • means H_2O molecules as ligands; b) Configuration of OH^- anion; c) Total charges of system; d) In unit of kcal·mol^{-1}; e) In unit of cm^{-1}.

Table 2. Selected interatomic distances (Å) at B3LYP/DZV level.

States	Mn-Mn	Mn_a-O	Mn_b-O	O-O	Mn_a-OH
1	2.724	1.781/1.755	2.016/2.019	2.593	
2	2.755	1.782/1.759	2.032/2.034	2.590	
3	2.652	1.790/1.785	1.784/1.790	2.397	
4	2.677	1.795/1.795	1.808/1.811	2.412	
5	2.639	1.873/1.799	1.803/1.767	2.438	1.884
6	2.666	1.977/1.771	1.799/1.810	2.490	1.897
7	2.649	1.745/1.756	1.809/1.811	2.370	1.812
8	2.655	1.757/1.770	1.817/1.814	2.390	1.810
9	2.674	1.716/1.815	1.859/1.777	2.387	1.815
10	2.673	1.745/1.849	1.841/1.764	2.413	1.961
11	2.710	1.789/1.818	1.764/1.744	2.288	1.795
12	2.699	1.788/1.825	1.780/1.748	2.324	1.791
13	2.733	1.764/1.913	1.785/1.705	2.319	1.743
14	2.715	1.767/1.928	1.798/1.706	2.366	1.741

Table 3. Mulliken spin populations of Mn atoms, oxo-atoms and OH ligands estimated at B3LYP/TZV//B3LYP/DZV level.

States	Mn_a	Mn_b	O	OH
1	–3.783	4.715	–0.005/0.052	
2	3.788	4.761	0.168/0.156	
3	3.796	–3.795	0.003/–0.004	
4	3.853	3.864	0.072/0.079	
5	3.791	–3.796	0.000/–0.012	0.034
6	3.831	3.844	0.160/0.026	0.032
7	–2.776	3.858	–0.108/–0.068	0.019
8	2.931	3.853	0.071/0.060	–0.002
9	–2.583	3.873	–0.209/–0.128	–0.073
10	2.814	3.841	0.093/0.118	0.110
11	2.974	–2.762	–0.060/–0.172	–0.030
12	2.982	2.902	0.025/0.047	0.019
13	2.684	–2.728	0.050/0.192	0.208
14	2.769	2.820	0.026/0.203	0.217

7, **8**, **9**, and **10** shown in **Table 1**. **Figure 3** shows the LS doublet states **7** and **9**. The corresponding HS octet states **8** and **10** have similar geometries to the LS states **7** and **9**. The optimized geometries retain the pseudo-octahedral configuration with Mn–Mn distances of 2.649 and 2.674 Å for **7** and **9**, respectively. The states **7** and **9** have similar Mn-O(OH^-) distances of 1.812 and 1.815 Å. From **Table 1**, the LS states are more stable by 4.4 and 0.3 kcal·mol^{-1} than the HS states for the axial and equatorial configurations, respectively. The axial state **7** is 13.7 kcal·mol^{-1} lower than the equatorial state **9**. The $\langle S^2 \rangle_{SC}$ values of **7** and **9** are, respectively, given by 3.0141 and 2.9857, indicating that three spins localized on both Mn atoms are antiferromagnetically coupled each other. From the spin densities shown in **Table 3**, single unpaired spin is localized on Mn_b atom. Thus, the oxidation states of two Mn atoms are apparently Mn_2(IV, III). The OH^- anion coordinates to Mn(IV) not Mn(III).

In the geometry of the LS doublet state **7**, the H-atom of the axial H_2O on Mn(III) ion faces to the O-atom of the OH ion, indicating the possibility that the H-atom of H_2O transfers to the OH bond to yield the Mn(III)-OH. **Figure 4** shows the energy change for the H-transfer from state **7**. The total energy increases and any local minimum or transition state was not found on the potential energy surface. The spin densities of both Mn atoms do not change to maintain the oxidation states of Mn(IV) and Mn(III). At R_{OH} = 1.6 Å, H_2O and OH are formed on the Mn(IV) and Mn(III), respectively. We could not find the optimized geometries in which the OH^- anion coordinates to Mn(III). In other word, the OH^- anion selectively coordinates to the Mn(IV) ion in the case of Mn_2(III, IV).

The optimized states **11** - **14**, which correspond to S_2 derived form Mn_2(III,III) at S_0, are summarized in **Table 1**.

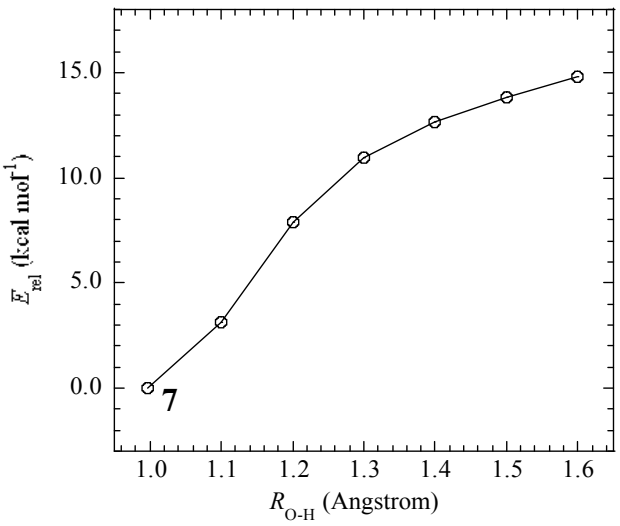

Figure 4. Energy change of H-transfer from H_2O coordinating to Mn_b to OH coordinating to Mn_a in the LS doublet state **7**. Relative energies are estimated at B3LYP/DZV level.

The geometries of the LS singlet states **11** and **13** shown in **Figure 3** are similar to **7** and **9**. Mn-Mn distances, 2.710 and 2.733 Å, close to 2.7 Å of the X-ray structure, are slightly longer than 2.649 and 2.674 Å of **7** and **9**. From the $\langle S^2 \rangle_{SC}$ –values and spin densities (**Table 3**), it is apparent that the oxidation state of Mn atoms are Mn_2(IV,IV) with three antiferromagnetic spin couplings. Similar to stabilities of **7** - **10**, the LS singlet state of axial configuration is more stable than that of equatorial configuration and the LS states are more stable than the corresponding HS state.

In summary, OH^- anion can coordinate to the Mn(IV) ion rather than the Mn(III) ion with retaining the octahedral geometry. It is reasonable that this result will be retained in the OEC. Thus, It is expected that the OH^- anion produced through the oxidation of water molecules coordinates to the Mn(IV) ion in the [Mn(μ-O)$_2$Mn] plane of the OEC in axial configuration.

3.2. S_3 States from Mn_2(III, II) at S_0

The geometries were fully optimized for all possible configurations of the coordination of two OH^- anions and all possible spin states. All optimized states of the S_3 states derived from Mn_2(III, II) and Mn_2(III, III) at S_0 are, respectively, summarized in **Tables S1** and **S2**. The states with the oxo-ligand, which are previously discussed in ref. 49, are also listed in both Tables. The selected configurations are summarized in **Table 4**. Two lowest configurations in energy and oxo-ligation are selected for the S_3 state from Mn_2(III, II) at S_0 and three lowest configurations for the S_3 state from Mn_2(III, III) at S_0 are selected. **Tables 5** and **6** summarize the selected interatomic distances and spin densities, respectively.

As shown in **Table 4**, the LS singlet state **15** with *t*-(a, a) configuration of two OH^- anions is most stable in energy. The corresponding HS septet state **16** is higher by only 0.8 kcal·mol^{-1}, consistent with small *J*-value of –42 cm^{-1} shown in **Table 4**. As can be seen from **Figure 5**, the optimized geometry has pseudo-octahedral configuration with the Mn–Mn distance of 2.654 Å slightly shorter than the observed 2.7 Å in OEC. It is found from $\langle S^2 \rangle_{SC}$ = 3.0719 shown in **Table 4** that three antiferromagnetic spin couplings exist in the LS singlet state **15**. From **Table 6**, the spin densities of Mn atoms are 2.897 e and –2.877 e, indicating that the oxidation states of Mn atoms are Mn_2(IV, IV). Since the charge densities of two OHs are respectively given by –0.351 and –0.343 e with the spin densities of –0.002 and 0.015 e, two OHs are apparently OH^- anions. The Mn-OH distances of 1.788 and 1.798 Å are comparable with 1.795 Å of **11** with the Mn_2(IV, IV) spin configuration (see **Tables 2** and **5**).

The second lowest LS singlet state **17** (**Table 4** and **Figure 5**) has the *c*-(a, a) configuration with 4.7 kcal·mol^{-1} higher than **15**. The singlet state **17** is a Mn_2(IV, IV)

Table 4. Oxidation states, spin angular momentums and relative energies of the optimized S_3 states at B3LYP/TZV//B3LYP/DZV level.

States	Ligands[a]	Conf.[b]	Charges[c]	Spin states	Oxidation states	$\langle S^2 \rangle_{SC}$	ΔE_{rel}[d]	$J_{Mn\text{-}Mn}$[h]
			S_3 states from Mn_2(III, II) at S_0					
15	(OH, OH)	*t*-(a, a)	2	Singlet	(IV, IV)	3.0719	0.0	−42
16		*t*-(a, a)	2	Septet	(IV, IV)	0.1265	0.8	
17[e]	(OH, OH)	*c*-(a, a)	2	Singlet	(IV, IV)	3.0886	4.7	−35
18		*c*-(a, a)	2	Septet	(IV, IV)	0.1308	5.4	
37	(O, •)	(a, •)	2	Singlet	(IV, IV)	3.0615	17.3	6
38		(a, •)	2	Septet	(IV, IV)	0.0936	17.0	
			S_3 states from Mn_2(III, III) at S_0					
19[g]	(O, •)	(a, •)	3	Doublet	(IV, IV)	2.7755	0.0	−110
20[g]		(a, •)	3	Sextet	(IV, IV)	0.8325	1.7	
21[g]		(a, •)	3	Doublet	(IV, IV)	2.9704	5.3	
22[g]		(a, •)	3	Octet	(IV, IV)	0.1045	8.2	
23	(OH, OH)	*t*-(a, a)	3	Doublet	(IV, IV)	3.0258	5.5	−170
24			3	Octet	(IV, IV)	0.0936	5.7	
25			3	Sextet	(IV, IV)	1.1397	11.2	
26	(OH, OH)	*c*-(a, a)	3	Sextet	(IV, IV)	0.9821	6.9	−128
27			3	Doublet	(IV, IV)	2.9083	8.3	
28			3	Octet	(IV, IV)	0.1467	15.7	

a) Symbol • means H_2O molecules as ligands; b) Configuration of OH^- anions and oxo atom; c) Total charges of system; d) In unit of kcal·mol^{-1}; e) Same as **15** shown in ref. 48; f) Same as **1** and **2** shown in ref. 48; g) Same as **7**, **8**, **9** and **10** shown in ref. 48; h) In unit of cm^{-1}.

Table 5. Selected interatomic distances (Å) at B3LYP/DZV level.

States	Mn-Mn	Mn_a-O	Mn_b-O	O-O	Mn_a-OH	Mn_b-OH	Mn_a-O
15	2.654	1.777/1.780	1.779/1.760	2.355	1.788	1.798	
16	2.649	1.780/1.784	1.786/1.765	2.375	1.793	1.799	
17	2.641	1.779/1.776	1.777/1.766	2.353	1.742	1.787	
18	2.644	1.783/1.782	1.780/1.769	2.365	1.737	1.788	
37	2.632	1.838/1.840	1.729/1.721	2.375			1.645
38	2.634	1.833/1.834	1.734/1.726	2.379			1.650
19	2.710	1.794/1.812	1.757/1.742	2.295			1.678
20	2.695	1.795/1.816	1.772/1.747	2.331			1.692
21	2.723	1.789/1.834	1.780/1.731	2.299			1.748
22	2.706	1.775/1.836	1.814/1..731	2.339			1.754
23	2.761	1.815/1.758	1.891/1.778	2.334	1.818	1.766	
24	2.752	1.857/1.776	1.853/1.777	2.369	1.778	1.780	
25	2.772	1.880/1.793	1.856/1.767	2.361	1.766	1.838	
26	2.670	1.786/1.782	1.784/1.785	2.320	1.844	1.848	
27	2.670	1.776/1.773	1.774/1.774	2.288	1.874	1.838	
28	2.661	1.783/1.784	1.784/1.779	2.329	1.885	1.898	

Table 6. Mulliken spin populations of Mn atoms, oxo-atoms and OH ligands at B3LYP/TZV//B3LYP/DZV level.

States	Mn_a	Mn_b	O	OH_a	OH_b	O
15	2.897	–2.877	0.015/–0.044	–0.002	0.015	
16	2.947	2.927	0.043/0.039	0.019	0.012	
17	2.915	–2.877	–0.011/–0.029	–0.012	0.011	
18	2.928	2.920	0.036/0.044	0.042	0.021	
37	2.742	–2.651	–0.192/–0.220			0.255
38	2.674	2.756	0.109/0.128			0.339
19	–2.850	2.743	0.076/0.166			0.887
20	2.835	2.893	0.044/0.057			–0.829
21	2.769	–2.771	0.223/–0.205			0.926
22	2.782	2.890	0.193/0.092			0.993
23	2.715	–2.910	0.715/0.067	0.478	–0.060	
24	2.810	2.809	0.656/0.042	0.315	0.328	
25	2.951	3.109	–0.792/–0.010	0.086	–0.408	
26	2.977	2.979	0.020/0.011	–0.511	–0.528	
27	2.851	–2.882	0.021/0.022	0.426	0.546	
28	3.000	2.992	0.011/0.002	0.433	0.489	

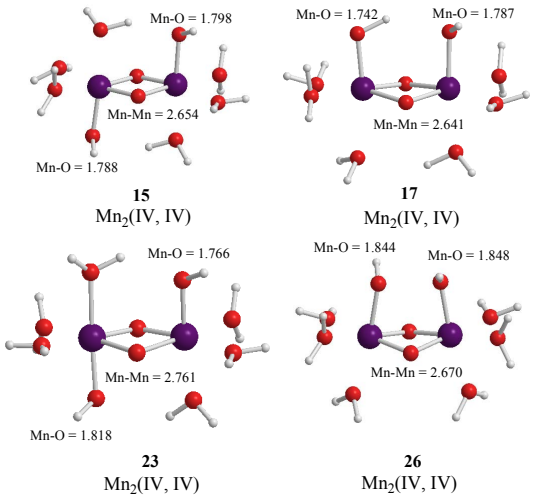

Figure 5. Optimized geometries of LS states in S_3 states derived from Mn_2(II,III) and Mn_2(III,III) at S_0. Mn-Mn and Mn-O(OH) distances are shown in unit of Å.

oxidation state that can be confirmed from $\langle S^2 \rangle_{SC}$ = 3.0886 and the spin densities of 2.915 and –2.877 e. This singlet state **17** is perfectly same as the singlet state **15** shown in our previous paper (ref. 49). As discussed in ref. 49, the state **17** is immediately formed from the singlet state **37** (**1** in ref. 49) that is a transient state on the potential energy surface and not a local minimum.

These S_3 states are produced by removing one proton and one electron from the S_2 states derived from Mn_2(III, II) at S_0, as shown in **Figure 1**. The most stable state **7** with the (a, •) configuration leads to the geometries **15** and **17** with formal Mn(III)-OH^- bond by removing one proton from the axial H_2O molecule on the Mn_b atom. Subsequently, one electron is removed from the Mn(III) ion to give a Mn(IV)-OH^- bond. This is reasonably consistent with fact that the OH^- anion does not coordinate to the Mn(III) ion as found for the states **7** - **10**, in **Table 1**. When one proton is removed from Mn(IV)-OH^- bond, the geometry **37** with Mn(IV) = O^{2-} bond is formed. The subsequent remove of one electron from another Mn(III) ion rather than the Mn(IV) ion occurs to give the singlet state **37**. As discussed above, this **37** is unstable and a transient state on the potential energy surface.

3.3. S_3 States from Mn_2(III, III) at S_0

The S_3 states under consideration corresponds to those in which one electron is removed from the S_3 states derived from Mn_2(III, II) at S_0 which are discussed in the preceding section. However the stabilities and electronic structures are significantly different from the preceding S_3 states. The most stable state is a LS doublet state **19** with axial configuration of oxo ligand in contrast with the *t*-(a, a) configuration of two OH^- anions in the singlet state **15**. The states, **19** - **22**, are perfectly same as the states, **7** - **10**, discussed in ref. 49. The oxidation states of Mn atoms in all states are Mn_2(IV, IV) and the Mn-O bond character is formally presented as Mn(IV)-O^-. **Figure 6** shows the magnetic orbitals MMO ∓ 3 corresponding to the Mn(IV)-O^- bond. These orbitals are composed of the in-phase and out-phase combinations of the bonding and antibonding orbitals of $3d_{yz}$(Mn) and $2p_y$(O). The bonding characters of both orbitals MMO ∓ 3 are due to the larger weight of the bonding orbital. **Table 7** summarizes the biradical indexes of the antiferromagnatically coupled orbitals. The biradical index of the MMO ∓ 3 is estimated to be 0.366, showing the definitely small bira- dical character, consistent with the bonding character of the MMO ∓ 3.

The second higher states in energy are states, **23** - **25**, in which two OHs coordinate to the Mn atoms with *t*-(a, a) configuration. The LS doublet state **23** is most stable among the *t*-(a, a) configurations with 5.5 kcal mol^{-1} higher than **19**. The $\langle S^2 \rangle_{SC}$ value is estimated to be 3.0258, showing that three sets of the antiferromagnetic

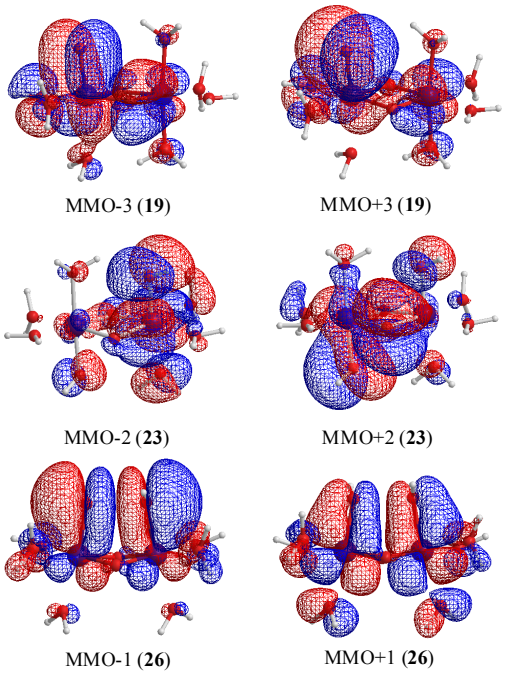

Figure 6. Magnetic orbitals in which anti-parallel spins couple antiferromagnetically.

Table 7. Biradical index and electron occupation numbers of antiferromagnetically coupled orbitals.

States	Orbitals	n_{-i}	n_{+i}	η_i^{BS}	η_i^{PBS}
19	MMO ∓ 3	1.569	0.431	0.752	0.366
20	MMO ∓ 1	1.547	0.453	0.772	0.398
23	MMO ∓ 2	1.201	0.799	0.971	0.890
25	MMO ∓ 1	1.221	0.779	0.965	0.868
26	MMO ∓ 1	1.433	0.567	0.860	0.572
27	MMO ∓ 3	1.428	0.572	0.863	0.579

spin coupling exist in the system. From the spin densities of two Mn atoms (2.715 and –2.910 e in **Table 6**), it is apparent that the oxidation state of Mn atoms is Mn_2(IV, IV).

In changing from S_2 to S_3 states through removes of one proton and one electron, it is natural to consider that each OH group is an anion and one electron is removed from Mn atom to yield Mn_2(IV, V). However, our results show that the oxidation state on Mn atoms is Mn_2(IV, IV) and one electron must be removed from OH^- anion or oxo atoms binding two Mn atoms. As can be confirmed from **Table 6**, the spin densities of oxo and OH_a anion are given to be 0.715 and 0.478 e, respectively. Their summation is equal to 1.193 e close to unity. **Figure 6** shows the MMO ∓ 2 that correspond to the antiferromagnetic spin coupling including contribution from oxo and OH_a anion. The orbital MMO + 2, which is occupied by a down-spin, is composed of the antibonding combi-

nation between the p_z orbital on oxo and lone pair orbital on OH_a. The MMO-2, which is occupied by a up-spin, distributes over the d_{yz} orbital on the Mn_b atom. The pure radical orbital (n = 1) is localized on another Mn_a atom. Thus, in the oxidation state of Mn_2(IV, IV) of the LS doublet state **23**, two spins on the Mn atoms are coupled antiferro-magnetically each other. The biradical index of the coupled orbitals MMO ∓ 2 is estimated to be 0.890 close to unity, showing the strong biradical character contrast with weak biradical character of the Mn(IV)-O^- bond.

As found in **Table 4**, the next higher energy state is **26** with the *c*-(a, a) configuration, which is only 1.2 kcal·mol^{-1} higher than the *t*-(a, a) configuration, **23**. However, the state **26** is a sextet state, in contrast with the doublet state **23**. The spin contamination $<S^2>_{SC}$ of the septet state **26** is given by 0.9821, indicating that one pair of the antiferromagnetic spin coupling exists in the system. From **Table 6**, the spin densities of 2.977 and 2.979 e of two Mn atoms shows that three spins are localized on each Mn atom. The spin densities of –0.511 and –0.528 e of two OH anions shows that single down-spin is delocalized over two OHs. It is expected that this down-spin is antiferromagnetically coupled with the up-spin of the Mn atoms.

The Mn-Mn distance of the sextet state **26** is estimated to be 2.670 Å longer by 0.029 Å than the singlet state **17** with same *cis* configuration and Mn_2(IV, IV). The Mn-OH distances are also longer than those of **17**. Although one OH forms a hydrogen bond to another OH in **17**, the O-O (in OH^- anions) distance of **26** is given by shorter 2.071 Å and two OHs make the face-to-face conformation. Then the state **26** has a slightly deformed pseudo-octahedral conformation, as can be seen from **Figure 5**.

Figure 6 shows the orbitals MMO ∓ 1 corresponding to the antiferromagnetic spin coupling, which were obtained by linear combination of the natural orbitals using the occupation numbers of 1.433 and 0.567. The MMO-1 is delocalized over two OHs in antibonding manner of the vertical lone pair orbitals of OH. The corresponding MMO + 1 is composed of the antibonding character of the d_{xz} orbitals on two Mn atoms. The lone pair orbital on OH is combined with the d_{xz} orbital on Mn atom in bonding character. As found from **Table 7**, the biradical index is estimated to be 0.572, showing the small biradical character contrast with the strong biradical index of 0.868 of the sextet state **25** with the *t*-(a, a) configuration. This small biradical character is consistent with bonding character of the lone pair orbital and d_{xz} orbital. In changing from S_2 to S_3 state, one electron is removed from the formed two OHs with retaining the oxidation state Mn_2 (IV, IV), not from the Mn atoms.

The doublet state **27** with the *c*-(a, a) configuration is 1.4 kcal mol^{-1} higher that the sextet state **26**. This state

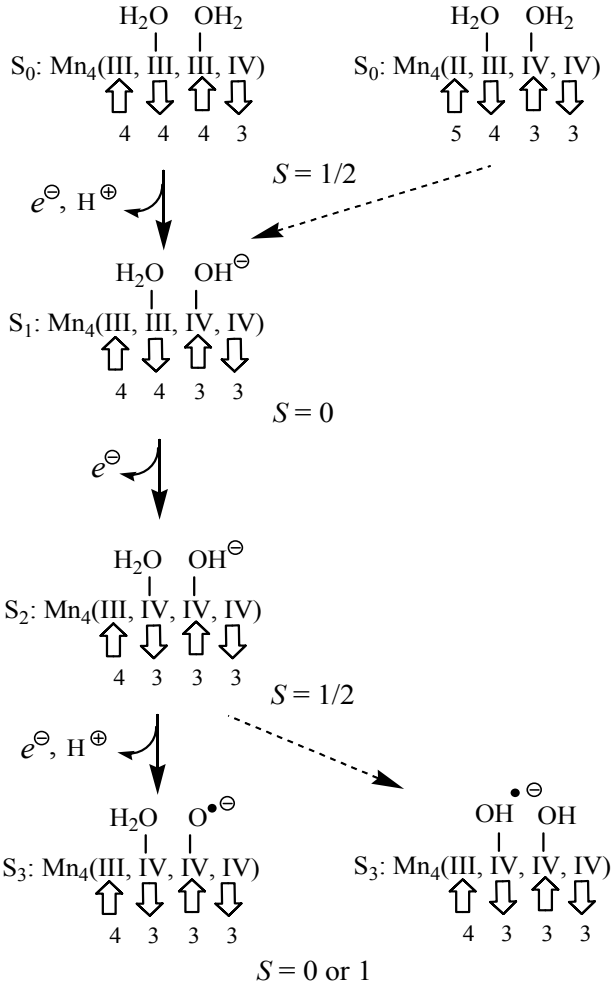

Figure 7. Proposal of reaction mechanism of oxidation of H_2O molecules from S_0 to S_3 states catalyzed by Mn cluster in OEC.

27 is perfectly same as the state **17** in ref. 49. As discussed in ref. 49, the state **27** is 8.3 kcal·mol^{-1} higher than the state **19** (**7** in ref. 49). The activation energy is estimated to be 14.2 kcal·mol^{-1} for the H-transfer from **19** to **27**.

4. Summary for OEC

The molecular and electronic structures of the model system, [Mn(μ-O)$_2$Mn], corresponding to the states from S_0 to S_3 along the Kok cycle, have been investigated using the density functional method. Several rules can be enumerated from our results in this study.

1) In the combination of Mn(II)-Mn(III), the Mn atoms do not keep the octahedral structure as can be seen from **Figure 3**. Accordingly, it is thought that the Mn(II) ion does not exist at the S_0 state in OEC.

2) In the combination of Mn(III)-Mn(III) coordinated by OH^- anion, the octahedral structure is remarkably deformed. In the Mn(III)-Mn(IV), the OH^- anion selectively coordinates to Mn(IV). Accordingly, it is thought that the OH^- anion coordinates to the Mn(IV) ion in OEC.

3) When the oxo atom directly bind to the Mn atom, the Mn atom must be a Mn(IV) ion.

It is possible from these results to propose the reaction mechanism of oxidation of two H_2O molecules from the S_0 to S_3 states in the OEC, as shown in **Figure 7**. It is known that the spin state of the S_2 state is a low spin state with S = 1/2 [60,61]. Following the reverse path from S_2 to S_0, it is considered that the spin state of the S_0 state is S = 1/2. Although it has been suggested that the oxidation states of the Mn atoms at the S_0 state are Mn_4(III, III, III, IV) and Mn_4(II, III, IV, IV), both have the spin state of S = 1/2 as can be seen form **Figure 7**. However, from above rule 1) the H_2O molecules coordinate to the Mn_2(III, IV) rather than the Mn_2(II, III) in the case of the Mn_4(II, III, IV, IV). Accordingly the Mn(II) ion cannot be considered to exist in OEC, indicating that the Mn_4(II, III, IV, IV) can be ruled out. In the Ferreira's structure [2], each Mn atom has rooms where the H_2O molecules occupy in octahedral configuration. Thus, the oxidation state at the S_0 state must be Mn_4(III, III, III, IV). It is considered that the H_2O molecule coordinated to Mn_2(III, III) plays an important role of the oxidation in OEC. Even if the Mn_4(II, III, IV, IV) exists in OEC, the H_2O molecules must coordinate to the Mn(III) and Mn(IV) ions of the Mn_4(II, III, IV, IV).

At the S_1 state, the OH^- anion is formed by removing a proton from the H_2O molecule. Since the formed OH^- anion selectively coordinates to the Mn(IV) ion from above rule 2) one electron is removed to yield the Mn(IV) ion from the Mn(III) ion coordinated by the H_2O molecule from which the proton is released. As shown in **Figure 4**, the reversible reaction, Mn(III)-OH_2 + Mn(IV)-OH^- $\rightleftarrows$ Mn(III)-OH^- + Mn(IV)-OH_2, does not definitely occur. The spin state of the S_1 state is given by $S = 0$, removing the up-spin from the Mn(III) ion.

The S_2 state is formed by removing one electron from the S_1 state. Judging from the change from **7** to **11**, one electron is not removed to yield the Mn(V)-OH^- from the Mn atom of the Mn(IV)-OH^-, but the Mn(IV)-OH_2 is formed by removing one electron from the Mn atom of Mn(III)-OH_2. Thus, the spin state changes from the singlet (S = 0) to doublet (S = 1/2) state.

Further releases of one electron and one proton lead to the S_3 state which is modeled by **19**, **23** and **26** in this text. The doublet state **19**, which is formed by change of Mn(IV)-OH^- → Mn(IV)-O^-, is more stable than the doublet **23** and sextet **26** states which have two OH^- anions. Since the doublet state **23** has *trans*-configuration of two OH, it is impossible that this conformation is put in the cubic Mn cluster of OEC. Although the sextet state **26** with the *cis*-configuration can be put in OEC, it is 6.9 kcal·mol^{-1} higher than **19**. Further problem is that the sextet state **26** has three spins on the Mn atoms in parallel alignment. The change from the S_2 to S_3 states does not continuously link due to the spin flipping. The doublet state **27** does not have the above problems, but the **27** has further high energy than the **26**. Accordingly it is thought that the Mn(IV)-O^- exists in the S_3 state.

In the changes from the S_0 to S_3 states, one of four Mn atoms plays important roles for four-electron oxidation of H_2O molecules in OEC. The Mn(IV)–O^- bond is formed by removing two protons and two electrons from the Mn(III)-OH_2. The possible spin state of the S_3 state is singlet or triplet. Considering that the O_2 molecule in the triplet state is produced, the spin state of the S_3 state would be triplet. Additionally the oxidation state of Mn(V) cannot be formed through the oxidation of H_2O molecules in OEC.

The problem which Mn atom of four atoms takes part in the oxidation has been left. In the Ferreira's structure [2], the Mn atom which is most close to Asp61 and linked by the hydrogen-bonding to Asp61 is the branching Mn atom of Mn-μO-Mn. Presumably, these two Mn atoms will be reactive, as shown in **Figure 7**. This year, the X-ray structure at resolution of 1.9 Å has been published [5]. Four Mn atoms are coordinated by ligands in octahedral configuration, while only one of four is coordinated by two H_2O molecules. The Ca ion is also coordinated by two H_2O molecules. One of two H_2O molecules on the Mn atom is hydrogen-bonded to one of two H_2O molecules on the Ca ion. These two hydrogen-bonded H_2O molecules might be substrates of formation of O_2 molecule. From the above rules, the oxidation state of four Mn atoms must be Mn_4(III, III, III, IV) at the S_0 state. It is expected that H_2O molecule on Mn atom is oxidized to yield the Mn(IV)-O^- bond at the S_3 state. This proposal for OEC at 1.9 Å resolution consistently matches with the results of our trial calculation using the structure at 1.9 Å resolution [62].

Another problem is a Ca ion in the cubic form of the catalytic site. It was proposed that it is involved in the oxidation mechanism of two H_2O molecules. Even if the Ca ion is involved in the oxidation mechanism, the H_2O molecule coordinated to the Ca ion might be oxidized at the stage of the S_4 state. However, the proposal for the Ca ion has not been established yet.

5. ACKNOWLEDGEMENTS

This work was supported by the Grant-in-Aid for Scientific Research (No. 22550010) from the Ministry of Education and Science, Japan. Y. Y of the authors would like to thank Prof. Kizashi Yamaguchi for providing the new structure of OEC and fruitful discussion.

REFERENCES

[1] Kok, B., Forbush, B. and McGloin, M. (1970) Cooperation changes in photosynthetic O_2 evolution-I. A linear

four step mechanism. *Photochemistry and Photobiology*, **11**, 457-475. doi:10.1111/j.1751-1097.1970.tb06017.x

[2] Ferreira, K.N., Iverson, T.M., Maghlaoui, K., Barber, J. and Iwata, S. (2004) Architecture of the photosynthetic oxygen-evolving center. *Science*, **303**, 1831-1838. doi:10.1126/science.1093087

[3] Loll, B., Kern, J., Saenger, W., Zouni, A. and Biesiadka, J. (2005) Towards complete cofactor arrangement in the 3.0 Å resolution structure of photosystem II. *Nature*, **438**, 1040-1044. doi:10.1038/nature04224

[4] Yano, J., Kern, J., Sauer, K., Latimer, M.J., Pushkar, Y., Biesiadka, J., Loll, B., Saenger, W., Messinger, J., Zouni, A. and Yachandra, V.K. (2006) Where water is oxidized to dioxygen: Structure of the photosynthetic Mn_4Ca cluster. *Science*, **314**, 821-825. doi:10.1126/science.1128186

[5] Umena, Y., Kawakami, K., Shen, J.-R. and Kamiya, N. (2010) Crystal structure of oxygen-evolving photosystem II at a resolution of 1.9 Å. *Nature*, **473**, 55-60. doi:10.1038/nature09913

[6] Robblee, J.H., Messinger, J., Cino, R.M., McFarlane, K.L., Fernandez, C., Pizzaro, S.A., Sauer, K. and Yachandra, V.K. (2002) The Mn cluster in the S_0 state of the oxygen-evolveing complex of photosystem II studied by EXAFS spectroscopy: Are there three di-μ-oxo-bridged Mn_2 moieties in the tetranuclear Mn complex? *Journal of the American Chemical Society*, **124**, 7459-7471. doi:10.1021/ja011621a

[7] Biesiadka, J., Loll, B., Kern, J., Irrgang, K.-D. and Zouni, A. (2004) Crystal structure of cyanobacterial photosystem II at 3.2 Å resolution: A close look at the Mn-cluster. *Physical Chemistry Chemical Physics*, **6**, 4733-4736. doi:10.1039/b406989g

[8] Yano, J., Pushkar, Y., Glatzel, P., Lewis A., Sauer, K., Messinger, J., Bergmann, U. and Yachandra, V.K. (2005) High-resolution Mn EXAFS of the oxygen-evolving complex in photosystem II: Structural implications for the Mn_4Ca cluster. *Journal of the American Chemical Society*, **127**, 14974-14975. doi:10.1021/ja054873a

[9] Debus R.J., Strickler M.A., Walker, L.M. and Hillier, W. (2005) No evidence from FTIR difference spectroscopy that asparatate-170 of the D1 polypeptide ligates a Manganese ion that undergoes oxidation during the S_0 to S_1, S_1 to S_2, or S_2 to S_3 transition in photosystem II. *Biochemistry*, **44**, 1367-1374. doi:10.1021/bi047558u

[10] Ono, T.-A., Noguchi, T., Inoue, Y., Kusunoki, M., Matsushita, T. and Oyanagi H. (1992) X-ray detection of the period-four cycling of the manganese cluster in photosynthetic water oxidizing enzyme. *Science*, **258**, 1335-1337. doi:10.1126/science.258.5086.1335

[11] Roelofs, T.A., Liang, W.C., Latimer, M.J., Cinco, R.M., Rompel, A., Andrews, J.C., Sauer, K., Yachandra, V.K. and Klein, M.P. (1996) Oxidation states of the manganese cluster during the flash-induced S-state cycle of the photosynthetic oxygen-evolving complex. *Proceedings of the National Academy of Sciences of the United States of America*, **93**, 3335-3340. doi:10.1073/pnas.93.8.3335

[12] Åhrling, K.A., Peterson, S. and Styring, S. (1997) An oscillating manganese electron paramagnetic resonance signal from the S_0 state of the oxygen evolving complex in photosystem II. *Biochemistry*, **36**, 13148-13152. doi:10.1021/bi971815w

[13] Messinger, J., Robblee, J.H., Yu, W.O., Sauer, K., Yachandra, V.K. and Klein, M.P. (1997) The S_0 state of the oxygen-evolving complex in photosystem II is paramagnetic: Detection of an EPR multiline signal. *Journal of the American Chemical Society*, **119**, 11349-11350. doi:10.1021/ja972696a

[14] Iuzzolino, L., Dittmer, J., Dörner, W., Meyer-Klaucke, W. and Dau, H. (1998) X-ray absorption spectroscopy on layered photosystem II membrane particles suggests manganese-centered oxidation of the oxygen-evolving complex for the S_0-S_1, S_1-S_2, and S_2-S_3 transitions of the water oxidation cycle. *Biochemistry*, **37**, 17112-17119. doi:10.1021/bi9817360

[15] Messinger, J., Robblee, J.H., Bergmann, U., Iuzzolino, L., Dorner, W., Meyer-Klaucke, W., Sole, V.A., Fernandez, C., Glatzel, H., Visser, R.M., Cinco, R.M., McFarlane, K.L., Bellacchio, E., Pizarro, S.A., Cramer, S.P., Sauer, K., Klein, M.P. and Yachandra, V.K. (2001) Absence of Mn-centered oxidation in the $S_2 \rightarrow S_3$ transition: implications for the mechanism of photosynthetic water oxidation. *Journal of the American Chemical Society*, **123**, 7804-7820. doi:10.1021/ja004307+

[16] Kulik, L.V., Epel, B., Lubitz, W. and Messinger, J. (2005) ^{55}Mn pulse ENDOR at 34 GHz of the S_0 and S_2 states of the oxygen-evolving complex in photosystem II. *Journal of the American Chemical Society*, **127**, 2392-2393. doi:10.1021/ja043012j

[17] Hallahan, B.J., Nugent, J.H., Warden, J. T. and Evans, M.C. (1992) Investigation of the origin of the "S3" EPR signal from the oxygen-evolving complex of photosystem 2: The role of tyrosine Z. *Biochemistry*, **31**, 4562-4573. doi:10.1021/bi00134a005

[18] Yachandra, V.K., Sauer, K. and Klein, M.P. (1996) Manganese cluster in photosynthesis: Where plants oxidize water to dioxygen. *Chemical Reviews*, **96**, 2927-2950. doi:10.1021/cr950052k

[19] Dau, H., Iuzzolino, L. and Dittmer, J. (2001) The tetramanganese complex of photosystem II during its redox cycle—X-ray absorption results and mechanistic implications. *Biochimica et Biophysica Acta*, **1503**, 24-39. doi:10.1016/S0005-2728(00)00230-9

[20] Robblee, J. H., Cinco, R. M. and Yachandra, V. K. (2001) X-ray spectroscopy-based structure of the Mn cluster and mechanism of photosynthetic oxygen evolution. *Biochimica et Biophysica Acta*, 2001, **1503**, 7-23. doi:10.1016/S0005-2728(00)00217-6

[21] Dau, H., Liebisch, M. and Haumann, M. (2003) X-ray absorption spectroscopy to analyze nuclear geometry and electronic structure of biological metal centers—Potential and questions examined with special focus on the tetra-nuclear manganese complex of oxygenic photosynthesis. *Analytical and Bioanalytical Chemistry*, **376**, 562-583. doi:10.1007/s00216-003-1982-2

[22] Dau, H. and Haumann, M. (2008) The manganese complex of photosystem II in its reaction cycle—Basic framework and possible realization at the atomic level. *Coordination*

Chemistry Reviews, **252**, 273-295. doi:10.1016/j.ccr.2007.09.001

[23] Goodson, P.A., Glerup, J., Hodgson, D.J., Michelsen, K. and Pedersen, E. (1990) Binuclear bis(μ-oxo)dimanganese (III,IV) and -(IV,IV) complexes with *N*,*N*'-bis(2-prydidylmethyl)-1, 2-ethanediamine. *Inorganic Chemistry*, **29**, 503-508. doi:10.1021/ic00328a034

[24] Pal, S., Gohdes, J.W., Wilisch, W.C.A. and Armstrong, W. H. (1992) Synthesis, structure, and properties of a complex that consists of an $[Mn_2O_2(O_2CCH_3)]^{2+}$ core and a spanning hexadentate ligand. *Inorganic Chemistry*, **31**, 713-716. doi:10.1021/ic00030a036

[25] Larson, E., Haddy, A., Kirk, M.L., Sands, R.H., Hatfield, W.E. and Pecoraro, V.L. (1992) The asymmetric mixed-valent complex $[Mn(2\text{-}OH\text{-}3,5\text{-}Cl_2\text{-}SALPN)]_2ClO_4$ shows a temperature-dependent interconversion between $g = 2$ mutiline and low-field EPR signals. *Journal of the American Chemical Society*, **114**, 6263-6265. doi:10.1021/ja00041a065

[26] Manchanda, R., Brudvig, G.W., de Gala, S. and Crabtree, R.H. (1994) Improved syntheses and structure of $[Mn^{III}Mn^{IV}(O)_2(phen)_4](Cl_4)_3{\bullet}2CH_3COOH{\bullet}2H_2O$. *Inorganic Chemistry*, **33**, 5157-5160. doi:10.1021/ic00100a049

[27] Baldwin, M.J., Stemmler, T.L., Riggs-Gelasco, P.J., Kirk, M.L., Penner-Hahn, J.E. and Pecoraro, V.L. (1994) Structural and magnetic effects of successive protonations of oxo bridges in high-valent manganese dimmers. *Journal of the American Chemical Society*, **116**, 11349-11356. doi:10.1021/ja00104a014

[28] Jensen, A.F., Su, Z., Hansen, N.K. and Larsen, F. K. (1995) X-ray diffraction study of the correlation between electrostatic potential and K-absorption edge energy in a bis(μ-oxo)Mn(III)-Mn(IV) dimer. *Inorganic Chemistry*, **34**, 4244-4252. doi:10.1021/ic00120a033

[29] Pal, S., Olmstead, M. M. and Armstrong, W. H. (1995) Syntheses, structures, and properties of $[Mn_2(\mu\text{-}O)_2(\mu\text{-}O_2CCH_3)(fac\text{-}bpea)_2](ClO_4)_2$ and two halide-ligated dioxo-bridged dimmers derived therefrom: $[Mn_2(\mu\text{-}O)_2X_2(mer\text{-}bpea)_2](ClO_4)_2$ (X = F, Cl). *Inorganic Chemistry*, **34**, 4708- 4715. doi:10.1021/ic00123a002

[30] Frapart, Y.-F., Boussac, A., Albach, R., Anxolabéhère-Mallart, E., Delroisse, M., Verlhac, J., Blondin, G., Girerd, J., Guilhem, J., Cesario, M., Rutherford, A.W. and Lexa, D. (1996) Chemical modeling of the oxygen-evolving center in plants. Synthesis, Structure and electronic and redox properties of a new mixed valence Mn-oxo cluster: $[Mn_2^{III,IV}O_2(bisimMe_2en)_2]^{3+}$ (bisimMe$_2$en = *N*,*N*'-dimethyl-*N*,*N*'-bis(imidazol-4-ylmetyl)ethane-1,2-diamine). EPR detection of an imidazole radical induced by UV irradiation at low temperature. *Journal of the American Chemical Society*, **118**, 2669-2678. doi:10.1021/ja9436411

[31] Horner, O., Charlot, M., Boussac, A., Anxolabéhère-Mallart, E., Tchertanov, L., Guilhem, J. and Girerd, J. (1998) Synthesis, structure, electronic, redox, and magnetic properties of a new mixed-valent Mn-oxo cluster: $[Mn_2^{III,IV}O_2$ (*N*,*N*bispicen)$_2]^{3+}$ (*N*,*N*bispicen = *N*,*N*-bis(2-pyridylmethyl)-1,2-diamino-ethane). *European Journal of Inorganic Chemistry*, 721-727. doi:10.1002/(SICI)1099-0682(199806)1998:6<721::AID-EJIC721>3.0.CO;2-H

[32] Schäfer, K., Bittl, R., Zweygart, W., Lendzian, F., Haselhorst, G., Weyhermüller, T., Wieghardt, K. and Lubitz, W. (1998) Electronic structure of antiferromagnetically coupled dinuclear manganese ($Mn^{III}Mn^{IV}$) complexes studied by magnetic resonance techniques. *Journal of the American Chemical Society*, **120**, 13104-13120. doi:10.1021/ja9827548

[33] Horner, O., Anxolabéhère-Mallart, E., Charlot, M., Tchertanov, L., Guilhem, J., Mattioli, T.A., Boussac, A. and Girerd, J. (1999) A new manganese dinuclear complex with phenolate ligands and a single unsupported oxo bridge. Storage of two positive charges within less than 500 mV. Relevance to photosynthesis. *Inorganic Chemistry*, **38**, 1222-1232. doi:10.1021/ic980832m

[34] Kirby, J.A., Robertson, A.S., Smith, J.P., Thompson, A.C., Cooper, S.R. and Klein, M.P. (1981) State of manganese in the photosynthetic apparatus. 1. Extended X-ray absorption fine structure studies on Chloroplasts and di-μ-oxo-bridged dimanganese model compounds. *Journal of the American Chemical Society*, **103**, 5529-5537. doi:10.1021/ja00408a042

[35] Penner-Hahn, J.E., Fronko, R.M., Pecoraro, V.L., Yocum, C.F., Betts, S.D. and Bowlby, N.R. (1990) Structural characterization of the manganese sites in the photosynthetic oxygen-evolving complex using X-ray absorption spectroscopy. *Journal of the American Chemical Society*, 1990, **112**, 2549-2557. doi:10.1021/ja00163a011

[36] Dismukes, G.C. and Siderer, Y. (1981) Intermediates of a polynuclear manganese center involved in photosynthetic oxidation of water. *Proceedings of the National Academy of Sciences of the United States of America*, **78**, 274-278. doi:10.1073/pnas.78.1.274

[37] Zhao, X.G., Richardson, W.H., Chen, J.-L., Li, J., Noodleman, L., Tsai, H.-L. and Hendrickson, D.N. (1997) Density functional calculations of electronic structure, charge distribution, and spin coupling in manganese-oxo dimer complexes. *Inorganic Chemistry*, **36**, 1198-1217. doi:10.1021/ic9514307

[38] Soda, T., Kitagawa, Y., Onishi, T., Takano, Y., Shigeta, Y., Nagao, H., Yoshioka, Y. and Yamaguchi, K. (2000) Ab initio computations of effective exchange integrals for H-H, H-He-H and Mn2O2 complex: Comparison of broken-symmetry approaches. *Chemical Physics Letters*, **319**, 223-230. doi:10.1016/S0009-2614(00)00166-4

[39] Delfs, C.D. and Stranger, R. (2001) Oxidation state dependence of the geometry, electronic structure, and magnetic coupling mixed oxo- and carboxylato-bridged manganese dimmers. *Inorganic Chemistry*, **40**, 3061-3076. doi:10.1021/ic0008767

[40] Sproviero, E.M., Gascon, J.A., McEvoy, J.P., Brudvig, G.W. and Batista, V.S. (2006) Characterization of synthetic oxo-manganese complexes and the inorganic core of the O_2-evolving complex in photosystem II: Evaluation of the DFT/B3LYP level of theory. *Journal of Inorganic Biochemistry*, **100**, 786-800. doi:10.1016/j.jinorgbio.2006.01.017

[41] Hasegawa, K. and Ono, T. (2006) Vibrational analyses of di-μ-oxo-bridged manganese dimers based on density functional theory calculations. Theoretical evaluation of Mn-O vibrations of the Mn-O cluster core for photosyn-

thetic oxygen-evolving complex. *Bulletin of the Chemical Society of Japan*, **79**, 1025-1031. doi:10.1246/bcsj.79.1025

[42] Ruiz-García, R., Pardo, E., Muñoz, M.C. and Cano, J. (2007) High valent bis(oxo)-bridged dinuclear manganese oxamates: Synthesis, crystal structures, magnetic properties, and electronic structure calculations of bis(μ-oxo)dimanganese(IV) complexes with binucleating *o*-phenylenedioxamate ligand. *Inorganica Chimica Acta*, **360**, 221-232.

[43] Orio, M., Pantazis, D.A., Petrenko, T. and Neese, F. (2009) Magnetic and spectroscopic properties of mixed valence manganese (III, IV) dimers: A sysnthetic study using broken symmetry density functional theory. *Inorganic Chemistry*, **48**, 7251-7260. doi:10.1021/ic9005899

[44] McGrady, J.E. and Stranger, R. (1997) Redox-induced changes in the geometry and electronic structure of di-μ-oxo-bridged manganese dimers. *Journal of the American Chemical Society*, **119**, 8512-8522. doi:10.1021/ja964360r

[45] McGrady, J.E. and Stranger, R. (1999) Redox-induced formation and cleavage of O-O and bonds in a peroxo-bridged manganese dimer: A density functional study. *Inorganic Chemistry*, **38**, 550-558. doi:10.1021/ic981253k

[46] Delfs, C.D. and Stranger, R. (2003) Investigating the stability of the peroxide bridge in (μ-oxo)- and bis(μ-oxo)manganese clusters. *Inorganic Chemistry*, **42**, 2495-2503. doi:10.1021/ic0205740

[47] Petrie, S. and Stranger, R. (2004) On the mechanism of dioxygen formation from a di-μ-oxo-bridged manganese dinuclear complex. *Inorganic Chemistry*, **43**, 5237-5244. doi:10.1021/ic049967k

[48] Mitani, M., Wakamatsu, Y., Katsurada, T. and Yoshioka, Y. (2006) Density functional study on geometrical features and electronic structures of di-μ-oxo bridged $[Mn_2O_2(H_2O)_8]^{q+}$ with Mn(II), Mn(III), and Mn(IV). *The Journal of Physical Chemistry A*, **110**, 13895-13914. doi:10.1021/jp0571877

[49] Katsuda, M., Hishikawa, E., Mitani, M. and Yoshioka, Y. (2010) Theoretical study of electronic structures of $[(H_2O)_3(O\text{-})Mn(m\text{-}oxo)_2Mn(OH_2)_4]^{q+}$ (q = 2 or 3) with Mn-O bond. *Physical Chemistry Chemical Physics*, **12**, 2730-2739. doi:10.1039/b914793d

[50] Proserpio, D.M., Hoffmann, R. and Dismukes, G.C. (1992) Molecular mechanism of photosynthetic oxygen evolution: A theoretical approach. *Journal of the American Chemical Society*, 1992, **114**, 4374-4382. doi:10.1021/ja00037a052

[51] Becke, A.D. (1993) Density—Functional thermochemistry III. The role of exact exchange. *Journal of Chemical Physics*, **98**, 5648-5652. doi:10.1063/1.464913

[52] Lee, C., Yang, W. and Parr, R.G. (1988) Development of Colle-Salvetti correlation-energy formula into a functional of the electron density. *Physical Review B*, **37**, 785-789. doi:10.1103/PhysRevB.37.785

[53] Schäfer, A., Horn, H. and Ahlrichs, R. (1992) Fully optimized contracted Gaussian basis sets for atoms Li to Kr. *Journal of Chemical Physics*, **97**, 2571-2577. doi:10.1063/1.463096

[54] Hariharan, P.C. and Pople, J.A. (1973) The influence of polarization functions on molecular orbital hydrogenation energies. *Theorefica Chimica Acta*, **28**, 213-222. doi:10.1007/BF00533485

[55] Schäfer, A., Huber, C. and Ahlrichs, R. (1994) Fully optimized contracted Gaussian basis sets of triple zeta valence quality for atoms Li to Kr. *Journal of Chemical Physics*, **100**, 5829-5835. doi:10.1063/1.467146

[56] Gaussian 03, Revision B.05, Frisch, M.J., Trucks, G.W., Schlegel, H.B., Scuseria, G.E., Robb, M.A., Cheeseman, J.R., Montgomery, Jr. J.A., Vreven, T., Kudin, K.N., Burant, J.C., Millam, J.M., Iyengar, S.S., Tomasi, J., Barone, V., Mennucci, B., Cossi, M., Scalmani, G., Rega, N., Petersson, G.A., Nakatsuji, H., Hada, M., Ehara, M., Toyota, K., Fukuda, R., Hasegawa, J., Ishida, M., Nakajima, T., Honda, Y., Kitao, O., Nakai, H., Klene, M., Li, X., Knox, J.E., Hratchian, H.P., Cross, J.B., Adamo, C., Jaramillo, J., Gomperts, R., Stratmann, R.E., Yazyev, O., Austin, A.J., Cammi, R., Pomelli, C., Ochterski, J.W., Ayala, P.Y., Morokuma, K., Voth, G.A., Salvador, P., Dannenberg, J.J., Zakrzewski, V.G., Dapprich, S., Daniels, A.D., Strain, M.C., Farkas, O., Malick, D.K., Rabuck, A.D., Raghavachari, K., Foresman, J.B., Ortiz, J.V., Cui, Q., Baboul, A.G., Clifford, S., Cioslowski, J., Stefanov, B.B., Liu, G., Liashenko, A., Piskorz, P., Komaromi, I., Martin, R.L., Fox, D.J., Keith, T., Al-Laham, M.A., Peng, C.Y., Nanayakkara, A., Challacombe, M., Gill, P.M.W., Johnson, B., Chen, W., Wong, M.W., Gonzalez, C. and Pople, J.A., Gaussian Inc., Pittsburgh, 2003.

[57] Amos, A.T. and Hall, G.G. (1961) Single determinant wave functions. *Proceedings of the Royal Society of London*, **263**, 483-493. doi:10.1098/rspa.1961.0175

[58] Liu, S. (2007) On the relationship between densities of Shannon entropy and fisher information for atoms and molecules. *Journal of Chemical Physics*, **126**, 1-3. doi:10.1063/1.2741244

[59] Mohajeri, A. and Alipour, M. (2009) Shannon information entropy of fractional occupation probability as an electron correlation measure in atoms and molecules. *Physical Chemistry*, **360**, 132-136. doi:10.1016/j.chemphys.2009.04.016

[60] Boussac, A., Sugiura, M., Rutherford, A.W. and Dorlet, P. (2009) Complete EPR spectrum of the S_3-state of the oxygen-evolving photsystem II. *Journal of the American Chemical Society*, **131**, 5050-5051. doi:10.1021/ja900680t

[61] Milikisiyants, S., Chatterjee, R., Weyers, A., Meenaghan, A., Coates, C. and Lakshmi, K.V. (2010) Ligand environment of the S_2 state of photosystem II: A study of the hyperfine interactions of the tetranuclear manganese cluster by 2D ^{14}N HYSCORE spectroscopy. *Journal of Physical Chemistry B*, **114**, 10905-10911. doi:10.1021/jp1061623

[62] Ichino, T., Yamaguchi, Y. and Yoshioka, Y. (2012) *Chemistry Letters*, **41**, 18-20. doi:10.1246/cl.2012.18

SUPPORTING MATERIALS

Contact to yyoshi.@chem.mie-u.ac.jp for Tables S1, S2, and S3.

Table S1. Oxidation states, spin angular momentums, total energies (hartree) and relative energies (kcal·mol^{-1}) of the optimized S_0 – S_3 states derived from Mn_2(II, III) at S_0 state.

Kok States	States	Ligands	Conf.	Charge	Spin States	Oxidation States	B3LYP/DZV			B3LYP/TZV//B3LYP/DZV		
							<S^2>	E_{total}	E_{rel}	<S^2>	E_{total}	E_{rel}
S_0	**1**	(•, •)		1	Doublet	(III, II)	4.7464	–3063.552296	0.0	4.7423	–3063.877108	0.0
	2	(•, •)		1	Decet	(III, II)	24.7981	–3063.548706	2.3	24.7962	–3063.873459	2.3
S_1	**5**	(OH, •)	(a, •)	1	Singlet	(III, III)	4.0118	–3062.961527	0.0	4.0029	–3063.288874	0.0
	6	(OH, •)	(a, •)	1	Nonet	(III, III)	20.0967	–3062.953946	4.8	20.0884	–3063.280003	5.6
		(OH, •)	(e, •)	1	Singlet	(III, III)	n.a	n.a	n.a	n.a	n.a	n.a
		(OH, •)	(e, •)	1	Nonet	(III, III)	n.a	n.a	n.a	n.a	n.a	n.a
S_2	**7**	(OH, •)	(a, •)	2	Doublet	(IV, III)	3.7769	–3062.611032	0.0	3.7641	–3062.933920	0.0
	8	(OH, •)	(a, •)	2	Octet	(IV, III)	15.8689	–3062.602923	5.1	15.8561	–3062.926919	4.4
	9	(OH, •)	(e, •)	2	Doublet	(IV, III)	3.7467	–3062.587688	14.6	3.7357	–3062.912052	13.7
	10	(OH, •)	(e, •)	2	Octet	(IV, III)	15.8542	–3062.585784	15.8	15.8436	–3062.911561	14.0
S_3	**15**	(OH, OH)	*t*-(a, a)	2	Singlet	(IV, IV)	3.0907	–3061.958582	0.0	3.0719	–3062.284790	0.0
	16	(OH, OH)	*t*-(a, a)	2	Septet	(IV, IV)	12.1431	–3061.956810	1.1	12.1265	–3062.283551	0.8
	17	(OH, OH)	*c*-(a, a)	2	Singlet	(IV, IV)	3.1085	–3061.952423	3.9	3.0886	–3062.277357	4.7
	18	(OH, OH)	*c*-(a, a)	2	Septet	(IV, IV)	12.1471	–3061.951017	4.7	12.1308	–3062.276161	5.4
	29	(2OH, •)	(ae, •)	2	Singlet	(IV, IV)	3.0542	–3061.949538	5.7	3.0424	–3062.276072	5.5
	30	(2OH, •)	(ae, •)	2	Septet	(IV, IV)	12.1166	–3061.948363	6.4	12.105	–3062.275143	6.1
	31	(2OH, •)	(aa, •)	2	Singlet	(IV, IV)	3.0828	–3061.947876	6.7	3.0682	–3062.275576	5.8
	32	(2OH, •)	(aa, •)	2	Septet	(IV, IV)	12.1133	–3061.948183	6.5	12.1028	–3062.276018	5.5
	33	(OH, OH)	(e, a)	2	Singlet	(IV, IV)	3.0521	–3061.942733	9.9	3.0401	–3062.269717	9.5
	34	(OH, OH)	(e, a)	2	Septet	(IV, IV)	12.1223	–3061.941058	11.0	12.1101	–3062.268307	10.3
	35	(OH, OH)	*t*-(e, e)	2	Singlet	(IV, IV)	3.0091	–3061.931055	17.3	3.0001	–3062.259339	16.0
	36	(OH, OH)	*t*-(e, e)	2	Septet	(IV, IV)	12.0983	–3061.928329	19.0	12.0891	–3062.256927	17.5
	37	(O, •)	(a, •)	2	Singlet	(IV, IV)	3.0724	–3061.934121	15.3	3.0615	–3062.257152	17.3
	38	(O, •)	(a, •)	2	Septet	(IV, IV)	12.1016	–3061.934637	15.0	12.0936	–3062.257756	17.0
	39	(OH, OH)	*c*-(e, e)	2	Singlet	(IV, IV)	2.9943	–3061.924557	21.4	2.9859	–3062.254505	19.0
	40	(OH, OH)	*c*-(e, e)	2	Septet	(IV, IV)	12.1084	–3061.922023	22.9	12.0976	–3062.252483	20.3
	41	(2OH, •)	(ee, •)	2	Singlet	(IV, IV)	3.0109	–3061.923654	21.9	3.0022	–3062.251210	21.1
	42	(2OH, •)	(ee, •)	2	Septet	(IV, IV)	12.1031	–3061.921004	23.6	12.0933	–3062.248996	22.5
	43	(O, •)	(e, •)	2	Singlet	(III, IV)	3.5489	–3061.922859	22.4	3.5192	–3062.247251	23.6
	44	(O, •)	(e, •)	2	Septet	(III, IV)	12.667	–3061.917703	25.7	12.6357	–3062.242597	26.5
	45	(O, •)	(e, •)	2	Triplet	(III, IV)	4.9743	–3061.900674	36.3	4.9687	–3062.225387	37.3
	46	(O, •)	(e, •)	2	Nonet	(III, IV)	20.0914	–3061.895560	39.5	20.0836	–3062.220960	40.1

Table S2. Oxidation states, spin angular momentums, total energies (hartree) and relative energies (kcal mol^{-1}) of the optimized S_0-S_3 states derived from Mn_3(III, III) at S_0 state.

Kok States	States	Ligands	Conf.	Charge	Spin States	Oxidation States	B3LYP/DZV			B3LYP/TZV//B3LYP/DZV		
							<S^2>	E_{total}	E_{rel}	<S^2>	E_{total}	E_{rel}
S_0	**3**	(•, •)		2	Singlet	(III, III)	4.0078	–3063.247881	0.0	3.9978	–3063.568593	0.0
	4	(•, •)		2	Nonet	(III, III)	20.098	–3063.235875	7.5	20.0887	–3063.557673	6.9
S_1	**7**	(OH, •)	(a, •)	2	Doublet	(IV, III)	3.7769	–3062.611032	0.0	3.7641	–3062.933920	0.0
	8	(OH, •)	(a, •)	2	Octet	(IV, III)	3.7769	–3062.602923	5.1	15.8561	–3062.926919	4.4
	9	(OH, •)	(e, •)	2	Doublet	(IV, III)	3.7467	–3062.587688	14.6	3.7357	–3062.912052	13.7
	10	(OH, •)	(e, •)	2	Octet	(IV, III)	15.8542	–3062.585784	15.8	15.8436	–3062.911561	14.0
S_2	**11**	(OH, •)	(a, •)	3	Singlet	(IV, IV)	3.0776	–3062.058404	0.0	3.0568	–3062.386461	0.0
	12	(OH, •)	(a, •)	3	Septet	(IV, IV)	12.1613	–3062.055821	1.6	12.1403	–3062.384369	1.3
	13	(OH, •)	(e, •)	3	Singlet	(IV, IV)	3.0003	–3062.038805	12.3	2.9908	–3062.367617	11.8
	14	(OH, •)	(e, •)	3	Septet	(IV, IV)	12.1187	–3062.035764	14.2	12.1061	–3062.364994	13.5
S_3	**19**	(O, •)	(a, •)	3	Doublet	(IV, IV)	3.5591	–3061.376971	0.0	3.5255	–3061.704662	0.0
	20	(O, •)	(a, •)	3	Sextet	(IV, IV)	9.6187	–3061.373722	2.0	9.5825	–3061.702025	1.7
	21	(O, •)	(a, •)	3	Doublet	(IV, IV)	3.7346	–3061.368148	5.5	3.7204	–3061.696229	5.3
	22	(O, •)	(a, •)	3	Octet	(IV, IV)	15.8669	–3061.363163	8.7	15.8545	–3061.691586	8.2
	23	(OH, OH)	*t*-(a, a)	3	Doublet	(IV, IV)	3.7951	–3061.366034	6.9	3.7758	–3061.695928	5.5
	24	(OH, OH)	*t*-(a, a)	3	Octet	(IV, IV)	15.8541	–3061.365569	7.2	15.8436	–3061.695657	5.7
	25	(OH, OH)	*t*-(a, a)	3	Sextet	(IV, IV)	9.9230	–3061.355494	13.5	9.8897	–3061.686861	11.2
	26	(OH, OH)	*c*-(a, a)	3	Sextet	(IV, IV)	9.7573	–3061.364224	8.0	9.7321	–3061.693738	6.9
	27	(OH, OH)	*c*-(a, a)	3	Doublet	(IV, IV)	3.6825	–3061.362223	9.3	3.6583	–3061.691486	8.3
	28	(OH, OH)	*c*-(a, a)	3	Octet	(IV, IV)	15.9202	–3061.349368	17.3	15.8967	–3061.679590	15.7
	47	(2OH, •)	(aa, •)	3	Doublet	(IV, IV)	3.7262	–3061.357648	12.1	3.7053	–3061.688068	10.4
	48	(2OH, •)	(aa, •)	3	Octet	(IV, IV)	15.8883	–3061.351253	16.1	15.8698	–3061.681845	14.3
	49	(2OH, •)	(aa, •)	3	Doublet	(IV, IV)	3.7977	–3061.353109	15.0	3.7744	–3061.681622	14.5
	50	(2OH, •)	(aa, •)	3	Sextet	(IV, IV)	9.8203	–3061.353528	14.7	9.7938	–3061.684444	12.7
	51	(2OH, •)	(ae, •)	3	Doublet	(IV, IV)	3.7710	–3061.357788	12.0	3.7575	–3061.687315	10.9
	52	(2OH, •)	(ae, •)	3	Octet	(IV, IV)	15.8822	–3061.354538	14.1	15.8667	–3061.684594	12.6
	53	(2OH, •)	(ae, •)	3	Doublet	(IV, IV)	3.8057	–3061.353521	14.7	3.7864	–3061.683410	13.3
	54	(2OH, •)	(ae, •)	3	Sextet	(IV, IV)	9.9056	–3061.350469	16.6	9.8841	–3061.680875	14.9
	55	(O, •)	(e, •)	3	Doublet	(IV, IV)	3.5113	–3061.357204	12.4	3.4668	–3061.686056	11.7
	56	(O, •)	(e, •)	3	Sextet	(IV, IV)	9.5873	–3061.352867	15.1	9.5471	–3061.682083	14.2
	57	(O, •)	(e, •)	3	Doublet	(IV, IV)	3.7604	–3061.341530	22.2	3.7455	–3061.670637	21.4
	58	(O, •)	(e, •)	3	Octet	(IV, IV)	15.8805	–3061.337059	25.0	15.8647	–3061.666532	23.9
	59	(OH, OH)	(e, a)	3	Doublet	(IV, IV)	3.7811	–3061.347572	18.4	3.7522	–3061.676244	17.8
	60	(OH, OH)	(e, a)	3	Sextet	(IV, IV)	9.8621	–3061.344763	20.2	9.8353	–3061.673895	19.3
	61	(OH, OH)	(e, a)	3	Doublet	(IV, IV)	3.8304	–3061.345638	19.7	3.8089	–3061.673804	19.4

Continued

62	(OH, OH)	(e, a)	3	Octet	(IV, IV)	15.9099	–3061.343117	21.2	15.8891	–3061.671753	20.7
63	(2OH, •)	(ee, •)	3	Doublet	(IV, IV)	3.7459	–3061.336991	25.1	3.7344	–3061.668173	22.9
64	(2OH, •)	(ee, •)	3	Octet	(IV, IV)	15.8931	–3061.333537	27.3	15.8754	–3061.665303	24.7
65	(2OH, •)	(ee, •)	3	Doublet	(IV, IV)	3.7726	–3061.330131	29.4	3.7541	–3061.661844	26.9
66	(2OH, •)	(ee, •)	3	Sextet	(IV, IV)	9.9116	–3061.326345	31.8	9.8894	–3061.658678	28.9
67	(OH, OH)	*t*-(e, e)	3	Doublet	(IV, IV)	3.7289	–3061.332295	28.0	3.7113	–3061.661216	27.3
68	(OH, OH)	*t*-(e, e)	3	Sextet	(IV, IV)	9.8265	–3061.329417	29.8	9.8061	–3061.658746	28.8
69	(OH, OH)	*t*-(e, e)	3	Doublet	(IV, IV)	3.7683	–3061.330593	29.1	3.7569	–3061.659151	28.6
70	(OH, OH)	*t*-(e, e)	3	Octet	(IV, IV)	15.8748	–3061.327770	30.9	15.8613	–3061.656696	30.1
71	(OH, OH)	*c*-(e, e)	3	Doublet	(IV, IV)	3.7196	–3061.327893	30.8	3.7045	–3061.656892	30.0
72	(OH, OH)	*c*-(e, e)	3	Sextet	(IV, IV)	9.8432	–3061.324672	32.8	9.8263	–3061.653946	31.8
73	(OH, OH)	*c*-(e, e)	3	Doublet	(IV, IV)	3.7611	–3061.326609	31.6	3.7508	–3061.655247	31.0
74	(OH, OH)	*c*-(e, e)	3	Octet	(IV, IV)	15.8757	–3061.323723	33.4	15.8625	–3061.652746	32.6

Table S3. Spin coupling constants (cm^{-1}) between Mn and Mn based on the geometries of the optimized LS states.

States	Ligands	Conf.	$J_{Mn\text{-}Mn}$	
			B3LYP/DZV	B3LYP/TZV//B3LP/DZV
1	(•, •)		–42	–41
3	(•, •)		–158	–150
5	(OH, •)	(a, •)	–112	–108
7	(OH, •)	(a, •)	–153	–142
9	(OH, •)	(e, •)	–159	–150
11	(OH, •)	(a, •)	–73	–68
13	(OH, •)	(e, •)	–88	–87
15	(OH, OH)	*t*-(a, a)	–48	–42
17	(OH, OH)	*c*-(a, a)	–41	–35
19	(O, •)	(a, •)	–114	–110
23	(OH, OH)	*t*-(a, a)	–180	–170
26	(OH, OH)	*c*-(a, a)	–129	–128
29	(2OH, •)	(ae, •)	–34	–31
31	(2OH, •)	(aa, •)	4	7
33	(OH, OH)	(e, a)	–48	–43
35	(OH, OH)	*t*-(e, e)	–69	–67
37	(O, •)	(a, •)	3	6
39	(OH, OH)	*c*-(e, e)	–73	–70
41	(2OH, •)	(ee, •)	–79	–75
43	(O, •)	(e, •)	–94	–92
47	(2OH, •)	(aa, •)	–60	–53
51	(2OH, •)	(ae, •)	–93	–89
55	(O, •)	(e, •)	–111	–108
59	(OH, OH)	(e, a)	–81	–75
63	(2OH, •)	(ee, •)	–99	–96
67	(OH, OH)	*t*-(e, e)	–81	–79
71	(OH, OH)	*c*-(e, e)	–91	–89